

Quantum Metric Length as a Fundamental Length Scale in Disordered Flat Band Materials

Chun Wang Chau^{1,3}, Tian Xiang¹, Shuai A. Chen^{1,2}, and K. T. Law¹

1. Department of Physics, Hong Kong University of Science and Technology, Clear Water Bay, Hong Kong, China
 2. Max Planck Institute for the Physics of Complex Systems, Nöthnitzer Straße 38, Dresden 01187, Germany and
 3. Cavendish Laboratory, Department of Physics, J J Thomson Avenue, Cambridge CB3 0HE, United Kingdom

(Dated: February 3, 2026)

Our previous understanding of electronic transport in disordered systems was based on the assumption that there is a finite Fermi velocity for the relevant electrons. The Fermi velocity determines important length scales in disordered systems such as the diffusion length and the localization length. However, in disordered systems with vanishing or nearly vanishing Fermi velocity, it is uncertain what determines the important length scales in such systems. In this work, we use the 1D Lieb lattice with isolated flat bands as an example to show that the quantum metric length (QML) is a fundamental length scale in the ballistic, diffusive and localization regimes. The QML is defined through the Bloch state wave functions of the flat bands. In the ballistic regime with short junctions, the QML controls the finite energy transport properties. In the localization regime with long junctions, the localization length is determined by the QML and remarkably, independent of disorder strength over a wide range of disorder strength. We call this unconventional localization regime, the quantum metric localization regime. In the diffusive regime, we demonstrate that the diffusion coefficient is linearly proportional to the QML via the wave-packet dynamics numerically. Importantly, the numerical results are consistent with the analytical results obtained through the Bethe-Salpeter equation. We conclude that the QML is a fundamentally important length scale governing the properties of disordered flat band materials.

Introduction— Flat-band systems, characterized by dispersionless energy bands, have emerged as a fertile platform for exploring diverse quantum phenomena, such as correlated insulating phases [1, 2], superconductivity [3–14], antiferromagnetism [15–17], and excitonic effects [18–20]. The quantum geometric tensor, which quantifies the phase and amplitude distances between quantum states [21–28], has emerged as a key quantity governing the physical properties of flat-band systems [12, 29–36]. Notably, recent studies suggest a connection between the quantum metric, the real part of the quantum geometric tensor, and the conductivity in flat bands with nontrivial quantum geometry [32–35, 37, 38].

To highlight an intriguing aspect of flat band disordered systems, we note that in conventional metals, the diffusion coefficient $D = v_F l$ is determined by the Fermi velocity v_F and the diffusion length $l = v_F \tau$ where τ is the scattering time. In this case, the conductivity is proportional to the diffusion coefficient [39]. For non-interacting flat bands, however, the vanishing Fermi velocity v_F suggests localization behavior [40]. The localization behavior can be altered by inelastic scatterings [32, 41, 42], defects [34, 43] and interactions [31, 44–48], which can potentially induce delocalization. Despite these efforts, some pivotal questions remain. First, as v_F goes to zero in flat band materials, what governs the characteristic length scales in the disordered regime? Second, are the diffusive and localized regimes in flat band materials fundamentally the same or different from the corresponding states in systems with large Fermi velocities?

In this work, we address the above questions by investigating disorder-driven quantum transport in flat-band materials with nontrivial quantum metric. Using the Landauer-Büttiker formalism [49–55], we study metal/flat-band/metal (M/FB/M) junctions based on Lieb lattice as shown in Fig. 1(c) and Fig. 2(a). By calculating the transmission probability between the two leads in the presence of disorder, we unveil

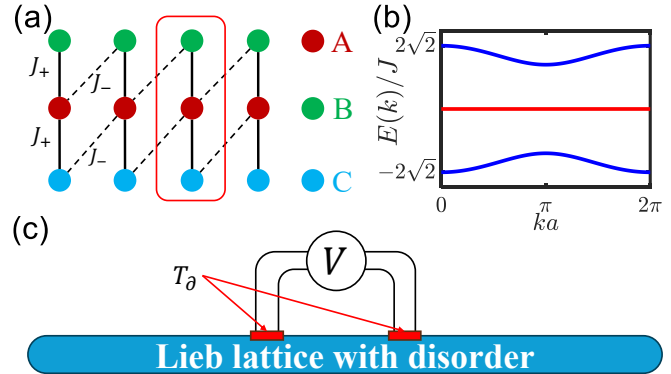


FIG. 1. (a) A 1D Lieb lattice, which contains three sub-lattices (A, B, and C, respectively) per unit cell. (b) A schematic band structure of a 1D Lieb lattice with an isolated flat band (red in color). (c) A schematic M/FB/M junction used to study the transport property of a Lieb lattice with disorder. The external leads are connected to the Lieb lattice with coupling strength T_d , and V denotes the voltage difference of the two leads.

the disorder-induced transport properties in isolated flat bands with quantum metric. First, in the clean limit, transmission at a finite energy is mediated by the interface states whose localization length is set by the quantum metric length (QML) as defined in Eq. (3). Second, disorders enable bulk-state transmission at zero energy as shown in Fig. 2(c). Thirdly, a highly conventional localization behavior is demonstrated for samples much longer than the QML and the localization length is determined by the QML as depicted in Fig. 2(e). Remarkably, the localization length is a constant, set by the QML, for a wide range of disorder strength. This is in sharp contrast to the Anderson localization regime in which the localization length decreases as the disorder strength increases. We call this regime, the quantum metric localization regime. Fourthly,

we observe a diffusive transport regime when the sample size is comparable with the QML as shown in Fig. 2(d). Furthermore, via wave-packet dynamics calculations, we show that the diffusion coefficient is linearly proportional to the QML as shown in Fig. 3. Interestingly, the diffusion coefficient is linearly proportional to disorder strength which contradicts the understandings from conventional theories. Importantly, we show that the numerical results are consistent with the results from the Bethe-Salpeter equation as summarized in Eq. (8). This work shows that the QML is the fundamental length scale in the flat band material in the ballistic, diffusive and localization regimes. Moreover, the diffusive and the localization regimes have anomalous dependence on the disorder strength.

Quantum Metric Length of Lieb Lattice Model — The M/FB/M junction for the study of disorder effects is constructed by connecting two metallic leads to a Lieb lattice as depicted in Fig. 1(a) and Fig. 2(a). In this section, we introduce the Lieb lattice with flat bands at the Fermi energy. First of all, each unit cell of the Lieb lattice hosts three sub-lattices (A, B, and C, respectively), with corresponding annihilation operators labeled as \hat{a}_x , \hat{b}_x , and \hat{c}_x , respectively. The Hamiltonian for a Lieb lattice reads $\hat{H}_{\text{Lieb}} = \sum_x \hat{h}_x$ with

$$\hat{h}_x = J_+ (\hat{b}_x^\dagger \hat{a}_x + \hat{c}_x^\dagger \hat{a}_x) + J_- (\hat{a}_x^\dagger \hat{b}_{x+1} + \hat{c}_x^\dagger \hat{a}_{x+1}) + \text{h.c.}, \quad (1)$$

where $J_{\pm} = J(1 \pm \delta)$ are the intra- and inter-cell hopping amplitudes respectively, and x labels the lattice site. The Lieb lattice features an isolated flat band which is separated from the two dispersive bands by a gap $\Delta = 2\sqrt{2}J\delta$ as illustrated in Fig. 1(b). The quantum metric for a Bloch state $|u(k)\rangle$ of the flat band with momentum k is defined as $\mathcal{G}(k) = \langle \partial_k u(k) | (1 - |u(k)\rangle \langle u(k)|) | \partial_k u(k) \rangle$. The Brillouin-zone average of the quantum metric of the flat band is given by

$$\bar{\mathcal{G}} = \frac{a}{2\pi} \int_{-\pi/a}^{\pi/a} \mathcal{G}(k) dk = \frac{a^2(1-\delta)^2}{8\delta}, \quad (2)$$

which has the dimension of length squared. The QML ℓ_{QM} is defined as:

$$\ell_{\text{QM}} = \bar{\mathcal{G}}/a, \quad (3)$$

where a is the lattice constant, and we set $a = 1$ throughout this work. Previous studies [29, 30, 56, 57] have shown that the QML determines the superconducting coherence length of the flat band superconductors [29, 30] and the localization length of topological bound states [56]. The question is, what is the role of the QML in disordered flat band systems when v_F goes to zero and important length scales such as the conventional diffusion length and the localization length vanish?

Disorder-free case — Before investigating the disordered cases, we first show the importance of the QML ℓ_{QM} without disorder. As depicted in Fig. 2(a) (lower panel), two metallic leads with bandwidth $2t_N$ are attached to the Lieb lattice and the Fermi energy is set at the flat band energy. The coupling

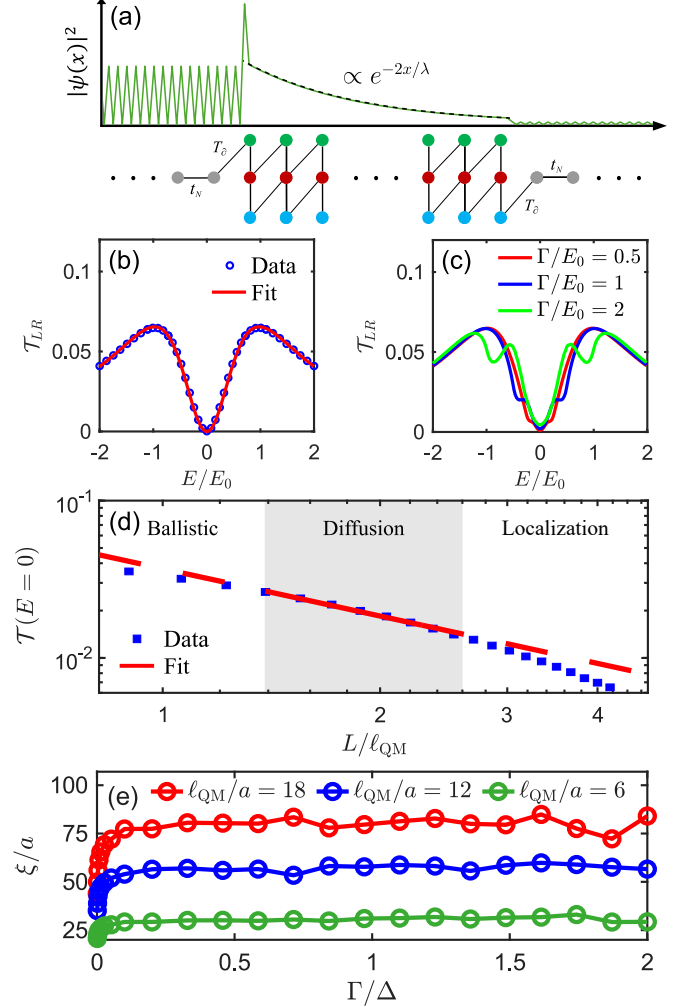


FIG. 2. (a) The $|\psi(x)|^2 = \sum_{\alpha=ABC} |\psi_{\alpha}(x)|^2$ of an interface state at the M/FB/M junction where $\psi_{\alpha}(x)$ is the α sub-lattice component of the wave function. Within the Lieb lattice, the probability density of $\psi_{\alpha}(x)$ decays exponentially away from the M/FB interface with a length scale $\lambda = 4\ell_{\text{QM}}$. (b) Transmission probability T_{LR} for a $L = 100$ junction without disorder with the setup of the lower panel of (a). No zero energy transmission is observed, and the transmission at finite energy is mediated by interface states with energy E_0 . (c) Zero energy transmission arises when disorder is introduced. (d) The transmission T at zero energy $E = 0$ for varying junction length L when $\Gamma/E_0 = 300$ with the setup illustrated in Fig. 1(c). Three distinct transport regimes are observed where the shaded region indicates the diffusive regime. The diffusive regime is characterized by the $1/L$ scaling, as depicted by the red dashed line. (e) The localization length ξ of the localization regime for varying disorder strength Γ for three sets of QML ℓ_{QM} . ξ increases in the weak disorder limit, reaching a plateau of $\xi \sim 4\ell_{\text{QM}}$ when disorder strength is comparable with the band gap Δ . The parameters in the calculations are chosen as $t_N = 1$, $J = 1000$, $\delta = 0.01$, $T_{\partial} = 0.1$, $E_0(\delta) = 4T_{\partial}^2\delta/t_N$ for (b-e).

amplitude between the lead and the Lieb lattice is denoted as T_{∂} . The transmission probability from the left lead to the right lead T_{LR} is calculated as $T_{LR} = \text{Tr}[\Gamma_L G^R \Gamma_R (G^R)^\dagger]$, where $\Gamma_{L/R}$ is the linewidth functions induced by the left and right

leads respectively, and G^R is the retarded Green's function of the lattice Hamiltonian \hat{H}_{Lieb} [53, 54, 58].

As shown in Fig. 2(b) for \mathcal{T}_{LR} versus E , where E is the energy difference between the leads' Fermi energy and the flat band energy of Lieb lattice, there is no zero energy transmission in the absence of disorders. This is consistent with the intuition that the conductance is zero when the Fermi velocity vanishes [40]. Interestingly, when the two metallic leads are coupled to the Lieb lattice, two interface states located at the M/FB and the FB/M interfaces are created. Importantly, the interface states have a decay length λ set by the QML as $\lambda = 4\ell_{\text{QM}}$ [58]. The probability density of an interface state $\psi(x)$ at M/FB interface is shown in Fig. 2(a) where x is the site index of the Lieb lattice. When the junction length is shorter or comparable with λ , the two left and right interface states hybridize to form a finite energy resonant state for electrons to tunnel through the junction. As a result, there are tunneling peaks at finite energy $E_0 = 4T_\partial^2\delta/t_N$ as depicted in Fig. 2(b). In the weak coupling limit, we can show analytically by two different methods [58] that the tunneling probability at energy E is given by

$$\mathcal{T}_{LR}(E) \approx \frac{16E^2E_0^2}{(E^2 + E_0^2)^2} e^{-\frac{2L}{\lambda}}. \quad (4)$$

The analytic expression of $\mathcal{T}_{LR}(E)$ (red curve in Fig. 2(b)) matches the numerical results nearly perfectly. It is important to note that the $\mathcal{T}_{LR}(E)$ is controlled by the length scale $\lambda = 4\ell_{\text{QM}}$ which clearly demonstrates the importance of the QML in the flat band materials in the clean limit.

Disorder effects and three transport regimes— To study the effects of disorder, we introduce Anderson-type onsite disorder to the Lieb lattice:

$$\hat{H}_{\text{dis}} = \sum_x w_x (\hat{a}_x^\dagger \hat{a}_x + \hat{b}_x^\dagger \hat{b}_x + \hat{c}_x^\dagger \hat{c}_x), \quad (5)$$

where the onsite potential w_x is independently and uniformly distributed in the range $[-\Gamma/2, \Gamma/2]$.

In the presence of disorder, the tunneling peaks near energy E_0 are smeared out as shown in Fig. 2(c). Importantly, finite transmission probability emerges at zero energy such that we have disorder enhanced electronic transport. Each data point in Fig. 2(c) for $\mathcal{T}_{LR}(E)$ is the average of results from 10000 disorder configurations. As the zero energy transport is away from the resonant state with energy E_0 , it is likely that the zero energy transmission is caused by the bulk transport as discussed below.

To understand the bulk state transport in the presence of disorder, we examine the dependence of the transmission on the sample size. Importantly, to minimize the contribution from the interface states as shown in Fig. 2(a), we connect the two metallic leads to the bulk of the Lieb lattice model as illustrated in Fig. 1(c). With the setup in Fig. 1(c), the zero energy transmission probability $\mathcal{T}(E = 0)$ as a function of junction length L is computed and the results are shown in Fig. 2(d). Interestingly, three distinct transport regimes are

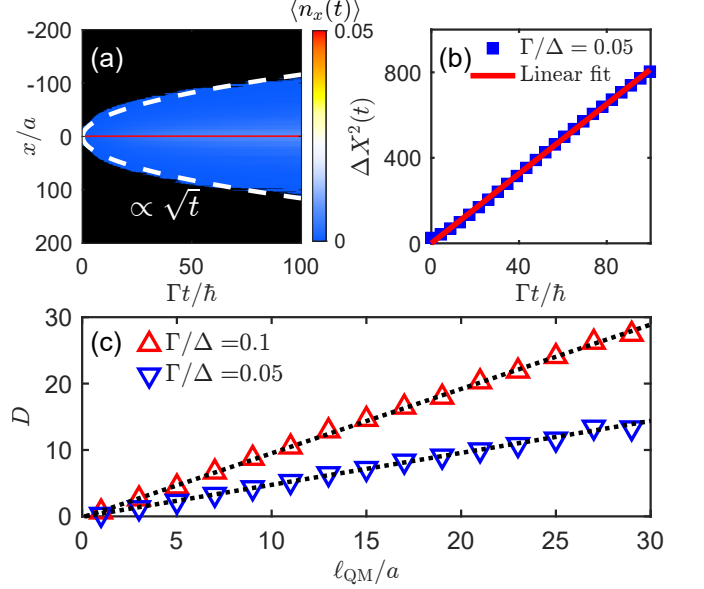


FIG. 3. (a) The time evolution of the site occupation $\langle n_x(t) \rangle = \langle \sum_\alpha |\psi_\alpha(x, t)|^2 \rangle$ for the wave packet $\psi(t)$, where $\psi(t = 0)$ is localized and projected to the flat band states. (b) The MSD $\Delta X^2(t)$ in (a). The simulation is performed with $\Gamma/\Delta = 0.05$. It is clear that $\Delta X^2(t) \propto 2Dt$ which indicates a diffusive behavior. (c) The linear fit of D as function of the QML ℓ_{QM} as predicted from Eq. (8), for disorder strengths $\Gamma/\Delta = 0.05$ and $\Gamma/\Delta = 0.1$ respectively. The simulation is performed on a 1D Lieb lattice with length $L = 401$ in (a-b) and $L = 1001$ in (c). All results are obtained by averaging over 500 disorder configurations.

observed depending on L . We identify the three transport regimes as the ballistic, diffusive and the localization regime, respectively.

For short junctions with $L < \ell_{\text{QM}}$, the transmission decreases linearly with length, following the relation $\mathcal{T} \propto 1 - L/\xi$ [59]. We identify this regime as the ballistic regime [60] ($L \ll \xi$) where ξ is in the order of the QML as shown in Fig. 2(d). On the other hand, for sufficiently long junctions ($L \gg \ell_{\text{QM}}$), the system transitions to the localized regime, where the transmission decays exponentially with L such that $\mathcal{T} \propto e^{-L/\xi}$ [61–63]. The localization lengths with different disorder strengths for long junctions are extracted through the calculations of $\mathcal{T} \propto e^{-L/\xi}$ and the results are shown in Fig. 2(e). It is interesting that the localization length *increases* as the disorder strength *increases* when Γ is small compared to the band gap Δ of the Lieb lattice in this weak disorder regime. This is in sharp contrast to the Anderson localization scenario when the localization length decreases as the disorder strength increases. Remarkably, as shown in Fig. 2(e), for a wide range of disorder strength in the order of Δ , the localization length is approximately close to $\lambda = 4\ell_{\text{QM}}$. We call this regime, the quantum metric localization regime where the localization length is determined by the QML and independent of disorder strength. This shows again that the QML is the important length scale in this unconventional localization regime.

When the junction length is comparable to the QML ℓ_{QM}

such that $L \approx \ell_{\text{QM}}$ [the shaded region in Fig. 2(d)], we have $\mathcal{T} \propto L^{-1}$ such that the Ohmic relation is satisfied [64]. The Ohmic relation is clearly shown by a straight line with slope -1 in the log-log plot of Fig. 2(d). In this regime, disorders disrupt the perfect interference that caused the formation of the exact flat band, allowing the electrons to propagate as in conventional disordered systems [65]. However, in conventional theories, the diffusion length is expected to be zero as the Fermi velocity is zero for a flat band. The question is, what is the length scale governing this diffusive transport regime? This question will be answered in the next section.

Wave packet dynamics calculations for the diffusion coefficient.— To further understand the properties of the diffusive transport regime, we study the short-time evolution of wavefunctions through the wave packet dynamics. In the wave packet dynamics, the diffusion coefficient can be extracted from the time dependent mean square displacement (MSD) $\Delta X^2(t)$ as $D = \frac{1}{2} \frac{d(\Delta X^2)}{dt}$, which can be calculated through [66–70]:

$$\Delta X^2(t) = \sum_{x=-L/2}^{L/2} x^2 \langle n_x(t) \rangle - \left(\sum_{x=-L/2}^{L/2} x \langle n_x(t) \rangle \right)^2, \quad (6)$$

where $\langle \cdot \rangle$ denotes the disorder average and $n_x(t) = \sum_{\alpha} |\psi_{\alpha}(x, t)|^2$ is the occupation number at site x at time t , and $\alpha \in (A, B, C)$ is the sublattice index. The MSD $\Delta X^2(t)$ measures how far the wave packet can spread over time. In particular, if the wave packet evolves diffusively, the MSD will grow linearly with time as $\Delta X^2(t) = 2Dt$ [66–69].

In Fig. 3(a), we start with a localized wave packet and project the wave function to the flat-band states [58, 71] to obtain an initial wavefunction $|\psi_0\rangle$. Then, the wave function evolves under the time-evolution operator such that $|\psi(t)\rangle = e^{-i\hat{H}t/\hbar}|\psi_0\rangle$, where \hat{H} contains Lieb lattice as well as the disorder term \hat{H}_{dis} . It is clear from Fig. 3(b) that the $\Delta X^2(t)$ scales linearly as a function of time, indicating that an initially localized wave packet diffuses via a random walk process [66, 72, 73]. If the initial localized state is projected to the dispersive bands, the $\Delta X^2(t)$ of the wave packet scales as t^2 instead as shown in the Supplemental Material [58], indicating the ballistic transport behavior in this weak disorder regime.

In Fig. 3(c), we further study the diffusive regime by tuning the QML, for two different disorder strengths. In particular, as the QML increases, the diffusion coefficient extracted from wave packet dynamics increases linearly accordingly. The results in Fig. 3 strongly indicate that the diffusion coefficient is linearly proportional to the QML in the diffusive regime. It is also clear that the diffusion coefficient increases as the disorder strength increases which is highly unconventional.

Solving the Bethe-Salpeter equation for the diffusion coefficient.— To have an analytical understanding of the observation that the diffusion coefficient is linearly proportional to the QML, we apply the diagrammatic techniques to obtain the diffusion coefficient through the Bethe-Salpeter equa-

tion [74, 75]. Employing the ladder approximation, the impurity vertex encapsulating the diffusion regime $\Pi(\omega, q)$ can be solved self-consistently:

$$\Pi(\omega, q) = \Pi_0(\omega, q) + P_0(\omega, q)\Pi_0(\omega, q)\Pi(\omega, q). \quad (7)$$

Here, $P_0(\omega, q)$ is the Fourier transform of $P_0(t, x, x')$ which is the probability to propagate from position x to x' in time t without collisions. On the other hand, $\Pi_0(\omega, q)$ is the bare impurity vertex, describing a single scattering process due to disorder. For a conventional dispersive band, the impurity vertex takes the form $\Pi(\omega, q) \propto 1/(-i\omega + Dq^2)$ [74–76], with $D = v_F l$ identified as the diffusion coefficient.

For the flat band case, the bare impurity vertex takes the form $\Pi_0(\omega, q) = \int \frac{dk}{2\pi} |\langle u(k) | u(k+q) \rangle|^2$, which reduces to $\Pi_0(\omega, q) \approx \Gamma^2(1 - q^2 \bar{G})$ in the small q limit. The diffusion probability without collisions is given by $P_0(\omega, q) = \bar{G}(E)\bar{G}(E + \omega)$, where $\bar{G}(E) \sim 2/(E + i\Gamma/\sqrt{3})$ is the disorder-averaged Green's function for $E \ll \Gamma$. In this case, solving Eq. (7) gives rise to the full impurity vertex $\Pi(\omega, q) \propto \frac{1}{-i\omega + C\Gamma\bar{G}q^2}$. The flat band impurity vertex [58] has the form as the dispersive band case and we can identify the diffusion coefficient as:

$$D = C \times \Gamma \ell_{\text{QM}} a. \quad (8)$$

The results reveal that for the flat band system, the diffusion coefficient scales linearly with the QML ℓ_{QM} . Incredibly, Eq. (8) is in agreement with the numerical results depicted in Fig. 3(c). Eq. (8) is significant as it generally applies to 1D systems with isolated flat bands and is not limited to the Lieb lattice chosen in the numerical studies. The proportionality constant $C \approx 0.337$ has been extracted numerically for the 1D Lieb lattice using data displayed in Fig. 3(c).

Discussion and conclusion.— In this work, using the 1D Lieb lattice, we demonstrate that the QML is the fundamental length scale governing the transport properties of flat band materials in the ballistic, diffusive as well as the localization regimes. Importantly, a highly unconventional quantum metric localization regime was identified in which the localization length is determined by the QML and independent of the disorder strength. Another unconventional diffusive regime was identified in which the diffusion constant is linearly proportional to the QML as well as the disorder strength. Using the Bethe-Salpeter equation, the numerical results in the diffusion regime were verified. The analytical result goes beyond the Lieb lattice and it generally applies to 1D lattices with isolated flat bands. In the future, more works will be needed to further establish the importance of QML in disordered flat band materials with other models [77].

In realistic materials such as in twisted bilayer graphene [78–80], the energy bands are generally dispersive. We expect that our results still apply when the QML is longer than the length scales introduced by the Fermi velocity. Furthermore, one important and natural extension of the current work

is to generalize the study to two-dimensional flat band materials. Due to the absence of Fermi velocity related length scales, we believe that the QML still plays an important role in two-dimensional flat band systems. As the QML can also be defined in electronic, photonic and phononic systems, our results are can be easily extended to photonic and phononic systems as well [81–85].

We thank Patrick A. Lee, Tai-Kai Ng, Carlo Beenakker, Roderich Moessner, Akito Daido, Sen Mu, and Haijing Zhang for their valuable discussions. K. T. L. acknowledges the support of the Ministry of Science and Technology, China, and the Hong Kong Research Grants Council through Grants No. MOST23SC01-A, No. RFS2021-6S03, No. C6025-19G, No. AoE/P-701/20, No. 16310520, No. 16310219, No. 16307622, and No. 16309223. K.T.L. is also supported by the New Cornerstone Investigator Program.

* These authors contributed equally to this work

† chsh@ust.hk

‡ phlaw@ust.hk

- [1] Yuan Cao, Valla Fatemi, Ahmet Demir, Shiang Fang, Spencer L. Tomarken, Jason Y. Luo, Javier D. Sanchez-Yamagishi, Kenji Watanabe, Takashi Taniguchi, Efthimios Kaxiras, Ray C. Ashoori, and Pablo Jarillo-Herrero, “Correlated insulator behaviour at half-filling in magic-angle graphene superlattices,” *Nature (London)* **556**, 80–84 (2018), arXiv:1802.00553 [cond-mat.mes-hall].
- [2] Emma C. Regan, Danqing Wang, Chenhao Jin, M. Iqbal Bakti Utama, Beini Gao, Xin Wei, Sihan Zhao, Wenyu Zhao, Zuocheng Zhang, Kentaro Yumigeta, Mark Blei, Johan D. Carlström, Kenji Watanabe, Takashi Taniguchi, Sefaattin Tongay, Michael Crommie, Alex Zettl, and Feng Wang, “Mott and generalized Wigner crystal states in WSe₂/WS₂ moiré superlattices,” *Nature (London)* **579**, 359–363 (2020), arXiv:1910.09047 [cond-mat.mes-hall].
- [3] Yuan Cao, Valla Fatemi, Shiang Fang, Kenji Watanabe, Takashi Taniguchi, Efthimios Kaxiras, and Pablo Jarillo-Herrero, “Unconventional superconductivity in magic-angle graphene superlattices,” *Nature (London)* **556**, 43–50 (2018), arXiv:1803.02342 [cond-mat.mes-hall].
- [4] Xiaobo Lu, Petr Stepanov, Wei Yang, Ming Xie, Mohammed Ali Aamir, Ipsita Das, Carles Urgell, Kenji Watanabe, Takashi Taniguchi, Guangyu Zhang, Adrian Bachtold, Allan H. MacDonald, and Dmitri K. Efetov, “Superconductors, orbital magnets and correlated states in magic-angle bilayer graphene,” *Nature (London)* **574**, 653–657 (2019), arXiv:1903.06513 [cond-mat.str-el].
- [5] Ville A. J. Pyykkönen, Sebastiano Peotta, Philipp Fabritius, Jeffrey Mohan, Tilman Esslinger, and Päivi Törmä, “Flat-band transport and Josephson effect through a finite-size sawtooth lattice,” *Phys. Rev. B* **103**, 144519 (2021), arXiv:2101.04460 [cond-mat.quant-gas].
- [6] Ville A. J. Pyykkönen, Sebastiano Peotta, and Päivi Törmä, “Suppression of Nonequilibrium Quasiparticle Transport in Flat-Band Superconductors,” *Phys. Rev. Lett.* **130**, 216003 (2023), arXiv:2211.09483 [cond-mat.supr-con].
- [7] Kukka-Emilia Huhtinen, Jonah Herzog-Arbeitman, Aaron Chew, Bogdan A. Bernevig, and Päivi Törmä, “Revisiting flat band superconductivity: Dependence on minimal quantum metric and band touchings,” *Phys. Rev. B* **106**, 014518 (2022), arXiv:2203.11133 [cond-mat.supr-con].
- [8] A. Julku, T. J. Peltonen, L. Liang, T. T. Heikkilä, and P. Törmä, “Superfluid weight and Berezinskii-Kosterlitz-Thouless transition temperature of twisted bilayer graphene,” *Phys. Rev. B* **101**, 060505 (2020), arXiv:1906.06313 [cond-mat.mes-hall].
- [9] Long Liang, Tuomas I. Vanhala, Sebastiano Peotta, Topi Siro, Ari Harju, and Päivi Törmä, “Band geometry, Berry curvature, and superfluid weight,” *Phys. Rev. B* **95**, 024515 (2017), arXiv:1610.01803 [cond-mat.supr-con].
- [10] P. Törmä, L. Liang, and S. Peotta, “Quantum metric and effective mass of a two-body bound state in a flat band,” *Phys. Rev. B* **98**, 220511 (2018), arXiv:1810.09870 [cond-mat.supr-con].
- [11] Sebastiano Peotta and Päivi Törmä, “Superfluidity in topologically nontrivial flat bands,” *Nature Communications* **6**, 8944 (2015), arXiv:1506.02815 [cond-mat.supr-con].
- [12] Päivi Törmä, Sebastiano Peotta, and Bogdan A. Bernevig, “Superconductivity, superfluidity and quantum geometry in twisted multilayer systems,” *Nature Reviews Physics* **4**, 528–542 (2022), arXiv:2111.00807 [cond-mat.supr-con].
- [13] Leon Balents, Cory R. Dean, Dmitri K. Efetov, and Andrea F. Young, “Superconductivity and strong correlations in moiré flat bands,” *Nature Physics* **16**, 725–733 (2020).
- [14] Valerio Peri, Zhi-Da Song, B. Andrei Bernevig, and Sebastian D. Huber, “Fragile Topology and Flat-Band Superconductivity in the Strong-Coupling Regime,” *Phys. Rev. Lett.* **126**, 027002 (2021), arXiv:2008.02288 [cond-mat.supr-con].
- [15] Yanhao Tang, Lizhong Li, Tingxin Li, Yang Xu, Song Liu, Katayun Barmak, Kenji Watanabe, Takashi Taniguchi, Allan H. MacDonald, Jie Shan, and Kin Fai Mak, “Simulation of Hubbard model physics in WSe₂/WS₂ moiré superlattices,” *Nature (London)* **579**, 353–358 (2020).
- [16] Guorui Chen, Aaron L. Sharpe, Eli J. Fox, Ya-Hui Zhang, Shaoxin Wang, Lili Jiang, Bosai Lyu, Hongyuan Li, Kenji Watanabe, Takashi Taniguchi, Zhiwen Shi, T. Senthil, David Goldhaber-Gordon, Yuanbo Zhang, and Feng Wang, “Tunable correlated Chern insulator and ferromagnetism in a moiré superlattice,” *Nature (London)* **579**, 56–61 (2020), arXiv:1905.06535 [cond-mat.mes-hall].
- [17] Siqi Wu, Chenchao Xu, Xiaoqun Wang, Hai-Qing Lin, Chao Cao, and Guang-Han Cao, “Flat-band enhanced antiferromagnetic fluctuations and superconductivity in pressurized CsCr₃Sb₅,” *Nature Communications* **16**, 1375 (2025), arXiv:2404.04701 [cond-mat.supr-con].
- [18] Evgeny M. Alexeev, David A. Ruiz-Tijerina, Mark Danovich, Matthew J. Hamer, Daniel J. Terry, Pramoda K. Nayak, Seongjoon Ahn, Sangyeon Pak, Juwon Lee, Jung Inn Sohn, Maciej R. Molas, Maciej Koperski, Kenji Watanabe, Takashi Taniguchi, Kostya S. Novoselov, Roman V. Gorbachev, Hyeyon Suk Shin, Vladimir I. Fal’ko, and Alexander I. Taratkovskii, “Resonantly hybridized excitons in moiré superlattices in van der Waals heterostructures,” *Nature (London)* **567**, 81–86 (2019), arXiv:1904.06214 [cond-mat.mes-hall].
- [19] Pasqual Rivera, Hongyi Yu, Kyle L. Seyler, Nathan P. Wilson, Wang Yao, and Xiaodong Xu, “Interlayer valley excitons in heterobilayers of transition metal dichalcogenides,” *Nature Nanotechnology* **13**, 1004–1015 (2018).
- [20] Xuzhe Ying and K. T. Law, “Flat band excitons and quantum metric,” arXiv e-prints , arXiv:2407.00325 (2024), arXiv:2407.00325 [cond-mat.mes-hall].
- [21] J. P. Provost and G. Vallee, “Riemannian structure on manifolds of quantum states,” *Communications in Mathematical Physics* **76**, 289–301 (1980).

[22] J. Anandan and Y. Aharonov, “Geometry of quantum evolution,” *Phys. Rev. Lett.* **65**, 1697–1700 (1990).

[23] R. Resta, “The insulating state of matter: a geometrical theory,” *European Physical Journal B* **79**, 121–137 (2011), [arXiv:1012.5776 \[cond-mat.mtrl-sci\]](#).

[24] Tianyu Liu, Xiao-Bin Qiang, Hai-Zhou Lu, and X. C. Xie, “Quantum geometry in condensed matter,” *National Science Review* **12**, nwae334 (2025), [arXiv:2409.13408 \[cond-mat.mes-hall\]](#).

[25] Oliver Breach, Robert-Jan Slager, and F. Nur Ünal, “Interferometry of Non-Abelian Band Singularities and Euler Class Topology,” *Phys. Rev. Lett.* **133**, 093404 (2024), [arXiv:2401.01928 \[cond-mat.quant-gas\]](#).

[26] Wojciech J. Jankowski, Arthur S. Morris, Adrien Bouhon, F. Nur Ünal, and Robert-Jan Slager, “Optical manifestations and bounds of topological euler class,” *Phys. Rev. B* **111**, L081103 (2025).

[27] Nicola Marzari, Arash A. Mostofi, Jonathan R. Yates, Ivo Souza, and David Vanderbilt, “Maximally localized Wannier functions: Theory and applications,” *Reviews of Modern Physics* **84**, 1419–1475 (2012), [arXiv:1112.5411 \[cond-mat.mtrl-sci\]](#).

[28] Nicola Marzari and David Vanderbilt, “Maximally localized generalized Wannier functions for composite energy bands,” *Phys. Rev. B* **56**, 12847–12865 (1997), [arXiv:cond-mat/9707145 \[cond-mat.mtrl-sci\]](#).

[29] Shuai A. Chen and K. T. Law, “Ginzburg-Landau Theory of Flat-Band Superconductors with Quantum Metric,” *Phys. Rev. Lett.* **132**, 026002 (2024), [arXiv:2303.15504 \[cond-mat.supr-con\]](#).

[30] Jin-Xin Hu, Shuai A. Chen, and K. T. Law, “Anomalous Coherence Length in Superconductors with Quantum Metric,” [arXiv e-prints](#), [arXiv:2308.05686](#) (2023), [arXiv:2308.05686 \[cond-mat.supr-con\]](#).

[31] Ohad Antebi, Johannes Mtscherling, and Tobias Holder, “Drude weight of an interacting flat-band metal,” *Phys. Rev. B* **110**, L241111 (2024), [arXiv:2407.09599 \[cond-mat.str-el\]](#).

[32] Johannes Mtscherling and Tobias Holder, “Bound on resistivity in flat-band materials due to the quantum metric,” *Phys. Rev. B* **105**, 085154 (2022), [arXiv:2110.14658 \[cond-mat.mes-hall\]](#).

[33] Bruno Mera and Johannes Mtscherling, “Nontrivial quantum geometry of degenerate flat bands,” *Phys. Rev. B* **106**, 165133 (2022), [arXiv:2205.07900 \[cond-mat.mes-hall\]](#).

[34] G. Bouzerar, “Giant boost of the quantum metric in disordered one-dimensional flat-band systems,” *Phys. Rev. B* **106**, 125125 (2022), [arXiv:2205.06164 \[quant-ph\]](#).

[35] Shuai A. Chen, Roderich Moessner, and Tai Kai Ng, “Generalized Peierls Substitution for Wannier Obstructions: Response to Disorder and Interactions,” *Phys. Rev. Lett.* **135**, 116502 (2025), [arXiv:2503.09709 \[cond-mat.str-el\]](#).

[36] Jun-Won Rhim and Bohm-Jung Yang, “Singular flat bands,” *Advances in Physics X* **6**, 1901606 (2021), [arXiv:2012.04279 \[physics.optics\]](#).

[37] Yugo Onishi and Liang Fu, “Quantum weight: A fundamental property of quantum many-body systems,” *Physical Review Research* **7**, 023158 (2025), [arXiv:2406.06783 \[cond-mat.str-el\]](#).

[38] Alexander Kruchkov, “Quantum transport anomalies in dispersionless quantum states,” *Phys. Rev. B* **107**, L241102 (2023).

[39] Steven M. Girvin and Kun Yang, *Modern Condensed Matter Physics* (Cambridge University Press, 2019).

[40] Kukka-Emilia Huhtinen and Päivi Törmä, “Conductivity in flat bands from the Kubo-Greenwood formula,” *Phys. Rev. B* **108**, 155108 (2023), [arXiv:2212.03192 \[cond-mat.mes-hall\]](#).

[41] Johannes Mtscherling, “Longitudinal and anomalous Hall conductivity of a general two-band model,” *Phys. Rev. B* **102**, 165151 (2020), [arXiv:2008.11218 \[cond-mat.str-el\]](#).

[42] G. Bouzerar and D. Mayou, “Quantum transport in self-similar graphene carpets,” *Physical Review Research* **2**, 033063 (2020).

[43] G. Bouzerar and D. Mayou, “Quantum transport in flat bands and supermetallicity,” *Phys. Rev. B* **103**, 075415 (2021), [arXiv:2007.05309 \[cond-mat.mes-hall\]](#).

[44] Katharina Laubscher, Clara S. Weber, Maximilian Hünenberger, Herbert Schoeller, Dante M. Kennes, Daniel Loss, and Jelena Klinovaja, “RKKY interaction in one-dimensional flat-band lattices,” *Phys. Rev. B* **108**, 155429 (2023), [arXiv:2210.10025 \[cond-mat.mes-hall\]](#).

[45] Joseph G. Checkelsky, B. Andrei Bernevig, Piers Coleman, Qimiao Si, and Silke Paschen, “Flat bands, strange metals, and the Kondo effect,” [arXiv e-prints](#), [arXiv:2312.10659](#) (2023), [arXiv:2312.10659 \[cond-mat.str-el\]](#).

[46] Jeronimo G. C. Martinez, Christie S. Chiu, Basil M. Smitham, and Andrew A. Houck, “Flat-band localization and interaction-induced delocalization of photons,” *Science Advances* **9**, eadj7195 (2023), [arXiv:2303.02170 \[quant-ph\]](#).

[47] Julien Vidal, Benoît Douçot, Rémy Mosseri, and Patrick Baudin, “Interaction Induced Delocalization for Two Particles in a Periodic Potential,” *Phys. Rev. Lett.* **85**, 3906–3909 (2000), [arXiv:cond-mat/0005215 \[cond-mat.str-el\]](#).

[48] Julien Vidal, Rémy Mosseri, and Benoit Douçot, “Aharonov-Bohm Cages in Two-Dimensional Structures,” *Phys. Rev. Lett.* **81**, 5888–5891 (1998), [arXiv:cond-mat/9806068 \[cond-mat.mes-hall\]](#).

[49] Rolf Landauer, “Electrical resistance of disordered one-dimensional lattices,” *Philosophical Magazine* **21**, 863–867 (1970).

[50] M. Büttiker, “Four-terminal phase-coherent conductance,” *Phys. Rev. Lett.* **57**, 1761–1764 (1986).

[51] M. Büttiker, “Absence of backscattering in the quantum Hall effect in multiprobe conductors,” *Phys. Rev. B* **38**, 9375–9389 (1988).

[52] R. de Picciotto, H. L. Stormer, L. N. Pfeiffer, K. W. Baldwin, and K. W. West, “Four-terminal resistance of a ballistic quantum wire,” *Nature (London)* **411**, 51–54 (2001).

[53] Hua Jiang, Haiwen Liu, Ji Feng, Qingfeng Sun, and X. C. Xie, “Transport Discovery of Emerging Robust Helical Surface States in $Z_2=0$ Systems,” *Phys. Rev. Lett.* **112**, 176601 (2014), [arXiv:1403.3743 \[cond-mat.mes-hall\]](#).

[54] Brandon G. Cook, Peter Dignard, and Kálmán Varga, “Calculation of electron transport in multiterminal systems using complex absorbing potentials,” *Phys. Rev. B* **83**, 205105 (2011).

[55] Zhe Hou, Ya-Yun Hu, and Guang-Wen Yang, “Moiré pattern assisted commensuration resonance in disordered twisted bilayer graphene,” *Phys. Rev. B* **109**, 085412 (2024), [arXiv:2307.09587 \[cond-mat.mes-hall\]](#).

[56] Xingyao Guo, Xinglei Ma, Xuzhe Ying, and K. T. Law, “Majorana Zero Modes in Lieb-Kitaev Model with Tunable Quantum Metric,” [arXiv e-prints](#), [arXiv:2406.05789](#) (2024), [arXiv:2406.05789 \[cond-mat.supr-con\]](#).

[57] Zhong C. F. Li, Yuxuan Deng, Shuai A. Chen, Dmitri K. Efetov, and K. T. Law, “Flat Band Josephson Junctions with Quantum Metric,” [arXiv e-prints](#), [arXiv:2404.09211](#) (2024), [arXiv:2404.09211 \[cond-mat.supr-con\]](#).

[58] See Supplemental Material: I. Quantum geometry of the Lieb lattice; II. Interface state wave functions and the transmission; III. Green’s function calculations; IV. Kubo-Greenwood formula and conductivity in the clean limit; V. Diagrammatic calculations in the presence of disorder; VI. Numerical approaches and results.

[59] J. Feilhauer and M. Moško, “Quantum and Boltzmann transport

in a quasi-one-dimensional wire with rough edges,” *Phys. Rev. B* **83**, 245328 (2011), arXiv:1011.6193 [cond-mat.mes-hall].

[60] E. Abrahams, P. W. Anderson, D. C. Licciardello, and T. V. Ramakrishnan, “Scaling Theory of Localization: Absence of Quantum Diffusion in Two Dimensions,” *Phys. Rev. Lett.* **42**, 673–676 (1979).

[61] Yi-Yi Mao, Chao Zeng, Yue-Ran Shi, Fei-Fei Wu, Yan-Jun Xie, Tao Yuan, Wei Zhang, Han-Ning Dai, Yu-Ao Chen, and Jian-Wei Pan, “Transition from flat-band localization to Anderson localization: Realization and characterization in a one-dimensional momentum lattice,” *Phys. Rev. A* **109**, 023304 (2024).

[62] Chao Zeng, Yue-Ran Shi, Yi-Yi Mao, Fei-Fei Wu, Yan-Jun Xie, Tao Yuan, Wei Zhang, Han-Ning Dai, Yu-Ao Chen, and Jian-Wei Pan, “Transition from Flat-Band Localization to Anderson Localization in a One-Dimensional Tasaki Lattice,” *Phys. Rev. Lett.* **132**, 063401 (2024).

[63] Max Hörmann and Kai Phillip Schmidt, “Dynamic structure factor of Heisenberg bilayer dimer phases in the presence of quenched disorder and frustration,” *Phys. Rev. B* **102**, 094427 (2020), arXiv:2004.00565 [cond-mat.str-el].

[64] Zheyong Fan, José H. Garcia, Aron W. Cummings, Jose Eduardo Barrios-Vargas, Michel Panhans, Ari Harju, Frank Ortmann, and Stephan Roche, “Linear scaling quantum transport methodologies,” *Physics Reports* **903**, 1–69 (2021), arXiv:1811.07387 [cond-mat.mes-hall].

[65] C. W. J. Beenakker and H. van Houten, “Quantum Transport in Semiconductor Nanostructures,” *Solid State Physics* **44**, 1–228 (1991).

[66] Mirko Daumann and Thomas Dahm, “Anomalous diffusion, prethermalization, and particle binding in an interacting flat band system,” *New Journal of Physics* **26**, 063001 (2024), arXiv:2402.12180 [cond-mat.stat-mech].

[67] Troels Markussen, Riccardo Rinaldi, Mads Brandbyge, and Antti-Pekka Jauho, “Electronic transport through Si nanowires: Role of bulk and surface disorder,” *Phys. Rev. B* **74**, 245313 (2006), arXiv:cond-mat/0606600 [cond-mat.mes-hall].

[68] Zheng-Wei Zuo, Jing-Run Lin, and Dawei Kang, “Topological inverse Anderson insulator,” *Phys. Rev. B* **110**, 085157 (2024), arXiv:2408.15826 [cond-mat.mes-hall].

[69] Stefano Longhi, “Inverse Anderson transition in photonic cages,” *Optics Letters* **46**, 2872 (2021), arXiv:2106.00231 [physics.optics].

[70] Ilan T. Rosen, Sarah Muschinske, Cora N. Barrett, David A. Rower, Rabindra Das, David K. Kim, Bethany M. Niedzielski, Meghan Schuldt, Kyle Serniak, Mollie E. Schwartz, Jonilyn L. Yoder, Jeffrey A. Grover, and William D. Oliver, “Flat-Band (De)localization Emulated with a Superconducting Qubit Array,” *Physical Review X* **15**, 021091 (2025), arXiv:2410.07878 [cond-mat.mes-hall].

[71] Daniel Leykam, Sergej Flach, Omri Bahat-Treidel, and Anton S. Desyatnikov, “Flat band states: Disorder and nonlinearity,” *Phys. Rev. B* **88**, 224203 (2013), arXiv:1305.7287 [cond-mat.dis-nn].

[72] K. Kawa and P. Machnikowski, “Diffusion of excitations and power-law localization in strongly disordered systems with long-range coupling,” *Phys. Rev. B* **102**, 174203 (2020).

[73] Ilia Tutunnikov, Chern Chuang, and Jianshu Cao, “Coherent spatial control of wave packet dynamics on quantum lattices,” *The Journal of Physical Chemistry Letters* **14**, 11632–11639 (2023), <https://doi.org/10.1021/acs.jpclett.3c03047>.

[74] Eric Akkermans and Gilles Montambaux, *Mesoscopic Physics of Electrons and Photons*, 1st ed. (Cambridge University Press, 2007).

[75] Henrik Bruus and Karsten Flensberg, *Many-Body Quantum Theory in Condensed Matter Physics: An Introduction* (Oxford University Press, 2004).

[76] P.B. Allen, “Chapter 6 Electron Transport,” in *Contemporary Concepts of Condensed Matter Science*, Vol. 2 (Elsevier, 2006) pp. 165–218.

[77] Jun-Won Rhim and Bohm-Jung Yang, “Classification of flat bands according to the band-crossing singularity of Bloch wave functions,” *Phys. Rev. B* **99**, 045107 (2019), arXiv:1808.05926 [cond-mat.str-el].

[78] Rafi Bistritzer and Allan H. MacDonald, “Moiré bands in twisted double-layer graphene,” *Proceedings of the National Academy of Science* **108**, 12233–12237 (2011), arXiv:1009.4203 [cond-mat.mes-hall].

[79] Kevin P. Nuckolls and Ali Yazdani, “A Microscopic Perspective on Moiré Materials,” *arXiv e-prints*, arXiv:2404.08044 (2024), arXiv:2404.08044 [cond-mat.mes-hall].

[80] Pedro Alcázar Guerrero, Viet-Hung Nguyen, Jorge Martínez Romeral, Aron W. Cummings, José-Hugo Garcia, Jean-Christophe Charlier, and Stephan Roche, “Disorder-Induced Delocalization in Magic-Angle Twisted Bilayer Graphene,” *Phys. Rev. Lett.* **134**, 126301 (2025), arXiv:2401.08265 [cond-mat.mes-hall].

[81] Cheng-Yi Chen, En Li, Huilin Xie, Jianyu Zhang, Jacky Wing Yip Lam, Ben Zhong Tang, and Nian Lin, “Isolated flat band in artificially designed Lieb lattice based on macrocycle supramolecular crystal,” *Communications Materials* **5**, 54 (2024).

[82] Shiqiang Xia, Yi Hu, Daohong Song, Yuanyuan Zong, Liqin Tang, and Zhigang Chen, “Demonstration of flat-band image transmission in optically induced Lieb photonic lattices,” *Optics Letters* **41**, 1435 (2016).

[83] Mingu Kang, Linda Ye, Shiang Fang, Jhih-Shih You, Abe Levitan, Minyong Han, Jorge I. Facio, Chris Jozwiak, Aaron Bostwick, Eli Rotenberg, Mun K. Chan, Ross D. McDonald, David Graf, Konstantine Kaznatcheev, Elio Vescovo, David C. Bell, Efthimios Kaxiras, Jeroen van den Brink, Manuel Richter, Madhav Prasad Ghimire, Joseph G. Checkelsky, and Riccardo Comin, “Dirac fermions and flat bands in the ideal kagome metal FeSn,” *Nature Materials* **19**, 163–169 (2020), arXiv:1906.02167 [cond-mat.str-el].

[84] Yuge Chen, Juntao Huang, Kun Jiang, and Jiangping Hu, “Decoding flat bands from compact localized states,” *Science Bulletin* **68**, 3165–3171 (2023), arXiv:2212.13526 [cond-mat.str-el].

[85] Daniel Leykam, Joshua D. Bodyfelt, Anton S. Desyatnikov, and Sergej Flach, “Localization of weakly disordered flat band states,” *European Physical Journal B* **90**, 1 (2017), arXiv:1601.03784 [cond-mat.dis-nn].